American Mineralogist, Volume 88, pages 1025–1032, 2003

High-pressure crystal structure of kosmochlor, $NaCrSi_2O_6$, and systematics of anisotropic compression in pyroxenes

MARCUS J. ORIGLIERI,[1,*] ROBERT T. DOWNS,[1] RICHARD M. THOMPSON,[1] CAROLYN J.S. POMMIER,[2] M. BONNER DENTON,[2] AND GEORGE E. HARLOW[3]

[1]Department of Geosciences, University of Arizona, Tucson, Arizona 85721-0077, U.S.A.
[2]Department of Chemistry, University of Arizona, Tucson, Arizona 85721-0041, U.S.A.
[3]Department of Earth and Planetary Sciences, American Museum of Natural History, New York, New York 10024-5192, U.S.A.

ABSTRACT

The crystal structure of synthetic kosmochlor, $NaCrSi_2O_6$, was studied using single crystal X-ray diffraction at high pressure. A four-pin diamond anvil cell, with 4:1 methanol:ethanol pressure medium, was used to achieve pressures to 9.28 GPa. Unit-cell data were collected at 20 pressures, and intensity data were collected at 13 of these pressures. Fitting the *P-V* data to a third-order Birch-Murnaghan equation yields V_0 = 418.84(3) Å^3, K_0 = 134(1) GPa^{-1}, and K_0' = 2.0(3). Anisotropic compression was observed with unit strain axial ratios of 1:1.82:2.08. The CrO_6 octahedron has a bulk modulus K_0 = 90(16) GPa^{-1}, while the SiO_4 tetrahedron has K_0 = 313(55) GPa^{-1}, both with $K_0' \equiv$ 4. An o-type rotation of the O3-O3-O3 linkage was observed with pressure, with ∠O3-O3-O3 decreasing from 172.8(2)° to 166.1(7)°. Compression in kosmochlor is related to the stacking directions of distorted cubic closest packed O atom monolayers. Unit strain ellipsoids for diopside, hedenbergite, spodumene (*C*2/*c* and *P*2$_1$/*c*), $LiScSi_2O_6$ (*C*2/*c* and *P*2$_1$/*c*), clinoenstatite, orthoenstatite, and $Mg_{1.54}Li_{.23}Sc_{.23}Si_2O_6$ (*Pbcn* and *P*2$_1$*cn*) were generated and discussed in terms of closest packing systematics. A relationship between the anisotropy of compression of olivines and pyroxenes is established. A strategy to determine not only the direction of a stress field in deformed rocks, but also an estimate of the magnitude of stress is discussed in terms of comparing the anisotropy of olivine and pyroxene.

INTRODUCTION

Pyroxenes are important phases of the Earth's upper mantle, second only to olivine in volumetric distribution. The crystal chemistry of the pyroxenes is summarized by Cameron and Papike (1981), at various temperatures by Cameron et al. (1973), and at various pressures by Yang and Prewitt (2000). As pyroxenes are a major phase of the Earth, their elastic properties are necessary to model the seismic properties of the Earth. Orthopyroxene undergoes a phase transition to clinopyroxene in the upper mantle (Hugh-Jones et al. 1996). Thus, clinopyroxene is a major component of the mantle, storing Mg, Fe, Ca, Na, Al, and Cr. Terrestrial occurrences of kosmochlor, summarized by Anthony et al. (1995), demonstrate that chromium is incorporated into clinopyroxene in terrestrial systems. Extensive solid solution between jadeite ($NaAlSi_2O_6$) and kosmochlor has been examined in Burmese samples (Harlow and Olds 1987). Solid solutions of kosmochlor with diopside ($CaMgSi_2O_6$) have also been observed (Secco et al. 2002).

Kosmochlor was first named by Laspeyres (1897), who found a Ca-Mg-Cr silicate in residues left after dissolution of the Toluca iron meteorite. Despite having a mere 3.3 mg of material, Laspeyres determined Ca, Mg, Fe, Al, and Cr to be present. Based upon the green color of the mineral, and its meteoritic origin, he chose the name kosmochlor. Because the structure of kosmochlor was not known, and its chemistry poorly established, when Frondel and Klein (1965) found a chromium analog of jadeite, they assigned it the new name ureyite. Later, an X-ray study of an old specimen of kosmochlor from the Bonn Museum indicated the identity of kosmochlor with ureyite (Neuhaus 1967). Since the name kosmochlor had priority, the name ureyite was dropped in favor of kosmochlor (Morimoto 1988).

The crystal structure of kosmochlor was first determined by Clark et al. (1969) from synthetic material. They found *C*2/*c* symmetry, and demonstrated the complete ordering of Cr and Na at the M1 and M2 sites, respectively. The pyroxene topology consists of chains of edge-sharing M1 octahedra and single chains of tetrahedra, both running parallel to **c**. Both Clark et al. (1969) and Cameron et al. (1973) suggested that the Na in the M2 site is eight-coordinated, based upon Na-O bond lengths.

This study was undertaken to investigate the influence of the M1 and M2 cations in clinopyroxene at high pressure. Kosmochlor provides a useful $M2^{+1}M1^{+3}Si_2O_6$ alternative to $M2^{+2}M1^{+2}Si_2O_6$ pyroxenes of the *C*2/*c* structure type. While examining compression in kosmochlor, large anisotropy was noted in the unit strain ratios: 1:1.82:2.08. This is more anisotropic than forsterite 1:1.99:1.55 (Downs et al. 1996). While the well-known anisotropy of olivine has been correlated to the splitting of seismic waves in the mantle, pyroxene compression may be even more anisotropic. If pyroxenes are a major

* E-mail: marcus@geo.arizona.edu

component of the mantle, then an understanding of the anisotropy of the seismic velocities of the mantle based only on olivine is not sufficient, and should include a contribution from pyroxene.

EXPERIMENTAL METHODS

Harlow (1997) crystallized kosmochlor from powdered Na-Cr silicate glass in a muffle furnace at 800 °C for 96 hours. The composition of the starting material was obtained by microprobe: $Na_{.994}Ca_{.002}Cr_{.992}Fe_{.004}Ti_{.002}Si_{2.001}O_6$. We treated the kosmochlor as fully ordered $NaCrSi_2O_6$. A suitable crystal, measuring 90 μm × 70 μm × 60 μm, was selected based upon an examination of peak profiles. Typical peak widths were 0.15° in ω, ~0.05° broader than the peaks of other well-crystallized clinopyroxenes we have examined.

The crystal was examined with an automated Picker diffractometer operated at 45 kV and 40 mA, using unfiltered Mo$K\alpha$ radiation. The positions of 17 high-intensity peaks (9° < 2θ < 30°) were determined using a modification of the eight-peak centering technique of King and Finger (1979). In particular, the positions were determined by fitting both $K\alpha1$ and $K\alpha2$ profiles with Gaussian functions, resulting in an order of magnitude improvement in final cell parameters. Refined cell parameters constrained to monoclinic symmetry are given in Table 1. A half sphere of intensity data was collected under room conditions to 2θ ≤ 60°, using ω scans of 1° width, step size 0.025°, and 3 s per step counting times. The structure was refined on F with anisotropic displacement parameters using a modification of RFINE (Finger and Prince 1975) to $R_w = 0.031$. Structural data at room conditions are summarized in Table 2. These data have smaller errors than Clark et al. (1969) ($R_w = 0.047$), but otherwise compare favorably.

The kosmochlor crystal was loaded into a four-pin Merrill Basset type diamond cell with (1$\bar{1}$0) parallel to the cell axis. The diamond anvil culet size was 600 μm. A stainless steel gasket, 250 μm thick, pre-indented to 90 μm, with a hole diameter of 300 μm was used. The cell was loaded with the kosmochlor crystal and a small ruby fragment, and filled with 4:1 methanol:ethanol pressure medium. Ruby fluorescence spectra were collected and the positions of the R1 and R2 peaks were determined by fitting Lorentzian functions. Using the method of Mao et al. (1978), pressure was calculated from the fitted R1 and R2 peak positions with an estimated error of ±0.05 GPa.

During the initial series of experiments, the gasket failed at 7.78 GPa. The cell was reloaded with the same crystal, again with (1$\bar{1}$0) parallel to the cell axis, and the experiment was continued to 9.28 GPa, at which point the gasket failed and the crystal cracked. Cell parameters at pressure were determined by the eight-peak centering method described above and are compiled in Table 1.

Every accessible reflection allowed by $C2/c$ symmetry, up to 716 intensity data (2θ ≤ 60°), were collected at pressure, with ω scans of 1.25° width, in steps of 0.025°, and counting times of 10 s per step. These data reduced to ~300 symmetry-equivalent reflections. Reflections violating $C2/c$ symmetry were sought, but none with significant intensities were found. Absorption corrections for the Be seats and diamond anvils were made from an absorption correction profile of the diamond cell before loading. Structure factors were weighted by $\omega = [\sigma_F^2 + (pF)^2]^{-1}$, where σ_F was obtained from counting statistics and p chosen to insure normally distributed errors (Ibers and Hamilton 1974). Structural data were refined with isotropic displacement factors using a modified version of RFINE (Finger and Prince 1975) and are summarized in Table 3. R_w ranged from 0.031 to 0.063.

The color of kosmochlor changed from emerald-green to greenish blue during compression from 1 atm to 9.28 GPa. In order to characterize this change, optical absorption spectroscopy was employed, using a Spectral Instruments 400 Series UV-Vis Spectrophotometer through a fiber optic probe. To correct for the spectroscopic response of the tungsten lamp and fiber optics, a background was acquired through air. There was no significant contribution to the spectrum from components of the diamond cell or the pressure medium.

Bond lengths and angles were calculated using BOND91 software, modified after Finger and Prince (1975). Polyhedral volumes and quadratic elongations were obtained with XTALDRAW (Downs and Hall-Wallace 2003). SPEEDEN (Downs et al. 2002) software was used to generate procrystal electron density maps that were analyzed to determine the existence of bonds between Na and O3.

TABLE 1. Kosmochlor unit-cell data as a function of pressure

P(GPa)	a(Å)	b(Å)	c(Å)	β (°)	V(Å³)
0.0001*	9.5720(3)	8.7094(2)	5.2678(2)	107.498(3)	418.84(3)
1.14*	9.5439(10)	8.6831(15)	5.2517(7)	107.441(9)	415.20(9)
1.51	9.5328(6)	8.6740(9)	5.2453(4)	107.408(6)	413.86(5)
2.22*	9.5173(6)	8.6605(9)	5.2374(4)	107.349(6)	412.05(6)
2.24	9.5165(8)	8.6603(11)	5.2362(5)	107.360(8)	411.89(7)
3.07	9.4976(8)	8.6413(7)	5.2261(4)	107.258(7)	409.60(5)
3.53*†	9.4867(4)	8.6323(5)	5.2206(3)	107.221(4)	408.36(3)
4.39	9.4700(11)	8.6136(5)	5.2095(5)	107.164(9)	406.01(6)
5.05*	9.4562(8)	8.5997(4)	5.2016(3)	107.104(7)	404.29(5)
5.56	9.4429(14)	8.5849(8)	5.1929(6)	107.040(12)	402.48(8)
5.78*†	9.4350(3)	8.5780(3)	5.1894(3)	107.030(3)	401.58(3)
6.25*	9.4295(8)	8.5700(4)	5.1844(3)	106.999(7)	400.65(4)
6.77	9.4183(8)	8.5571(4)	5.1770(3)	106.947(7)	399.11(5)
7.08*	9.4110(6)	8.5517(3)	5.1729(2)	106.910(5)	398.32(3)
7.23*†	9.4105(4)	8.5481(3)	5.1727(2)	106.915(3)	398.10(3)
7.39*	9.4059(5)	8.5472(2)	5.1703(2)	106.892(4)	397.72(3)
7.40	9.4054(8)	8.5454(4)	5.1696(3)	106.889(7)	397.57(4)
8.50*†	9.3836(4)	8.5201(6)	5.1560(3)	106.776(5)	394.68(4)
8.97*†	9.3742(6)	8.5086(7)	5.1484(4)	106.721(6)	393.28(4)
9.28*†	9.3694(4)	8.5028(4)	5.1456(2)	106.717(3)	392.61(3)

* Intensity data collected at this pressure.
† Indicates second loading of cell.
Space group $C2/c$.

RESULTS AND DISCUSSION

A pressure-volume equation of state for kosmochlor was obtained by fitting the data from Table 1 to a third order Birch-Murnaghan equation, yielding $V_0 = 418.84(3)$ Å³, $K_0 = 134(1)$ GPa⁻¹, and $K_0' = 2.0(3)$. A plot of the data and the fitted curve are included in Figure 1.

A unit strain ellipsoid (Fig. 2) was generated for the change from 0.0001 GPa to 9.28 GPa using the STRAIN software by Ohashi (Hazen and Finger 1982). Compression ratios of the principal axes of the unit strain ellipsoid are 1:1.82:2.08. The middle value represents strain symmetrically constrained to lie parallel to **b**. The most compressible direction is approximately perpendicular to the plane ($\bar{3}$02), lying in the **a-c** plane, ~141° from **a**, while the most incompressible direction is ~(201). The orientation of the ellipsoid does not vary over the pressure range of this study. The values of the unit strain in both the most compressible direction [–0.002930(5)], and parallel to **b** [–0.002556(5)], remain invariant with pressure. However, the value of unit strain in the most incompressible direction steadily decreases with pressure from –0.0020(1) between 1 atm and 1.14 GPa to –0.001407(6) between 1 atm and 9.28 GPa. This

TABLE 2. Structural parameters for kosmochlor in air at room conditions

atom	x	y	z	B_{eq} (Å²)	β_{11}	β_{22}	β_{33}	β_{12}	β_{13}	β_{23}
Na2	0	0.2999(2)	_	1.55(4)	0.0051(3)	0.0045(3)	0.0122(8)	0	–0.0005(4)	0
Cr1	0	0.90769(9)	_	0.91(2)	0.00277(9)	0.0030(1)	0.0078(3)	0	0.0005(1)	0
Si	0.29259(9)	0.0918(1)	0.2343(2)	0.92(2)	0.0028(1)	0.0031(1)	0.0081(3)	0.0000(1)	0.0008(2)	0.0000(2)
O1	0.1137(3)	0.0784(3)	0.1366(5)	1.01(4)	0.0027(3)	0.0038(3)	0.0081(8)	–0.0002(2)	0.0004(4)	0.0004(4)
O2	0.3605(3)	0.2689(3)	0.3033(5)	1.25(4)	0.0038(3)	0.0039(3)	0.0123(9)	–0.0005(3)	0.0014(4)	–0.0001(4)
O3	0.3529(3)	0.0095(3)	0.0092(5)	1.14(4)	0.0035(3)	0.0040(3)	0.0097(8)	0.0006(3)	0.0014(4)	–0.0002(5)

Note: Space group = $C2/c$.

TABLE 3. Structural parameters for kosmochlor as a function of pressure

P (GPa)		1.14	2.22	3.53	5.05	5.78	6.25	7.08	7.23	7.39	8.50	8.97	9.28
obs refl		219	228	224	198	143	195	181	158	194	155	157	169
total refl		316	312	310	291	299	296	290	293	288	291	290	286
p^*		1.13	1.16	1.17	1.17	1.17	1.15	1.19	1.18	1.13	1.15	1.17	1.14
R_w		0.052	0.063	0.063	0.049	0.045	0.046	0.031	0.031	0.049	0.050	0.050	0.051
Cr	*y*	0.9082(2)	0.9079(3)	0.9084(3)	0.9088(3)	0.9091(5)	0.9087(3)	0.9088(3)	0.9086(3)	0.9089(3)	0.9092(5)	0.9096(5)	0.9094(3)
	B(iso)	1.23(4)	0.78(5)	0.93(4)	0.78(5)	0.76(7)	0.80(5)	0.84(5)	0.69(4)	0.77(5)	0.74(6)	0.83(6)	0.70(5)
Na	*y*	0.3006(6)	0.3005(7)	0.3020(7)	0.3031(7)	0.303(1)	0.3034(6)	0.3058(6)	0.3025(7)	0.3053(7)	0.303(1)	0.304(1)	0.3044(8)
	B(iso)	1.80(9)	1.5(1)	1.4(1)	1.5(1)	1.2(1)	1.3(1)	1.3(1)	1.2(1)	1.3(1)	1.2(1)	1.4(1)	1.2(1)
Si	*x*	0.2925(3)	0.2927(3)	0.2928(3)	0.2924(4)	0.2926(4)	0.2929(4)	0.2927(4)	0.2929(3)	0.2933(4)	0.2936(4)	0.2936(3)	0.2935(3)
	y	0.0921(3)	0.0922(3)	0.0922(3)	0.0936(4)	0.0934(6)	0.0935(3)	0.0936(3)	0.0933(4)	0.0934(3)	0.0932(5)	0.0938(5)	0.0933(4)
	z	0.2342(4)	0.2344(5)	0.2347(4)	0.2343(5)	0.2344(6)	0.2343(5)	0.2355(4)	0.2348(5)	0.2356(5)	0.2352(6)	0.2350(6)	0.2363(5)
	B(iso)	1.29(5)	0.92(5)	0.93(5)	0.95(6)	0.64(7)	0.86(6)	0.95(5)	0.70(5)	0.79(6)	0.77(7)	0.75(7)	0.72(6)
O1	*x*	0.1144(7)	0.1149(9)	0.1146(8)	0.116(1)	0.114(1)	0.115(1)	0.116(1)	0.1148(8)	0.116(1)	0.1136(9)	0.1142(9)	0.1142(8)
	y	0.0798(6)	0.0793(8)	0.0802(8)	0.0799(9)	0.082(1)	0.0805(7)	0.0813(7)	0.0820(9)	0.0812(8)	0.079(1)	0.080(1)	0.081(1)
	z	0.138(1)	0.136(1)	0.140(1)	0.139(1)	0.137(2)	0.138(1)	0.140(1)	0.141(1)	0.139(1)	0.138(1)	0.139(1)	0.138(1)
	B(iso)	1.34(9)	1.0(1)	1.2(1)	0.9(1)	0.8(1)	0.8(1)	0.8(1)	0.8(1)	0.9(1)	0.8(1)	0.8(1)	0.7(1)
O2	*x*	0.3614(7)	0.3606(9)	0.3604(8)	0.360(1)	0.362(1)	0.362(1)	0.362(1)	0.3588(8)	0.358(1)	0.360(1)	0.359(1)	0.3585(8)
	y	0.2583(7)	0.2585(8)	0.2605(8)	0.2611(8)	0.261(1)	0.2622(7)	0.2627(7)	0.2624(7)	0.2637(7)	0.264(1)	0.264(1)	0.264(1)
	z	0.306(1)	0.307(1)	0.308(1)	0.310(1)	0.314(2)	0.313(1)	0.313(1)	0.312(1)	0.311(1)	0.313(1)	0.314(1)	0.314(1)
	B(iso)	1.4(1)	1.1(1)	1.2(1)	1.0(1)	0.8(1)	1.1(1)	1.2(1)	0.8(1)	1.0(1)	1.0(1)	1.1(2)	0.9(1)
O3	*x*	0.3527(7)	0.3548(9)	0.3535(7)	0.359(1)	0.353(1)	0.354(1)	0.358(1)	0.3570(9)	0.358(1)	0.355(1)	0.357(1)	0.3560(8)
	y	0.0109(7)	0.0114(8)	0.0142(8)	0.0131(7)	0.0162(9)	0.0150(6)	0.0172(6)	0.0161(7)	0.0165(7)	0.017(1)	0.018(1)	0.0184(9)
	z	0.007(1)	0.008(1)	0.008(1)	0.005(2)	0.004(2)	0.002(2)	0.002(2)	0.003(1)	0.002(2)	0.002(2)	0.004(2)	0.000(1)
	B(iso)	1.45(9)	1.1(1)	0.9(1)	1.0(1)	0.8(1)	0.9(1)	1.07(9)	0.9(1)	0.9(1)	0.7(1)	0.8(1)	0.7(1)

Notes: *B*(iso) in Å^3; $x_{Cr} = x_{Na} = 0$; $z_{Cr} = z_{Na} = {}^1/_4$.
* Weights computed by $w = [\sigma_F^2 + p^2F^2]^{-1}$.

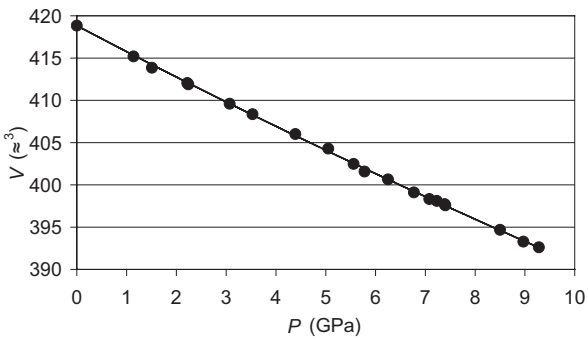

FIGURE 1. Variation of unit-cell volume with pressure for kosmochlor. Fitted curve is a third order Birch-Murnaghan equation, with $V_0 = 418.84(3)$ Å^3, $K_0 = 134(1)$ GPa^{-1}, and $K_0' = 2.0(3)$.

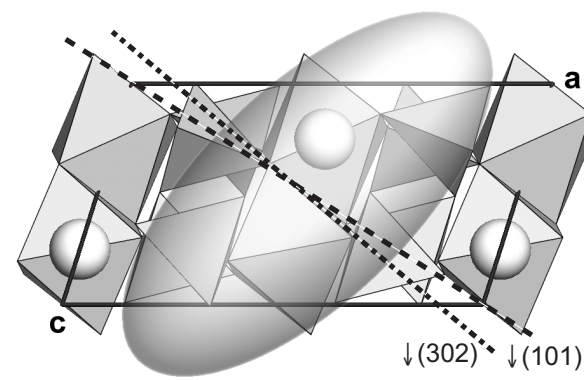

FIGURE 2. Oriented unit strain ellipsoid for kosmochlor overlying a cartoon of the kosmochlor structure viewed down **b**. CrO_6 and SiO_4 are depicted as polyhedra and Na as a sphere. The softest compression direction is parallel to the long axis of the ellipsoid and roughly parallel to $(\bar{3}02)$.

indicates that only compression in the stiffest direction significantly contributes to the pressure derivative of the bulk modulus.

Analysis of the procrystal electron density distribution indicates six bonds to the Na atom under room conditions (Downs 2003). Using the nomenclature of Burnham et al. (1967), Na is bonded to O1B1, O1A1, O2C2, O2D2, O3C1, and O3D1, as illustrated in Figure 3. These bonds are symmetrically related by the twofold symmetry axis through the Na atom; consequently there are three pairs of unique bonds. All Na-O bond distances decrease systematically, however R(Na-O1) and R(Na-O2) decrease at a rate ~1.7 times greater than R(Na-O3C1) [or equivalently, R(Na-O3D1)], as illustrated in Figure 4. Linear extrapolation indicates that R(Na-O3C2) and R(Na-O3C1) should have the same value at ~20 GPa. As pressure increases, the longer, initially nonbonded R(Na-O3C2) [or equivalently, R(Na-O3D2)] distance decreases at a rate ~7 times that of Na-O3C1, which should eventually lead to bonding of a fourth pair of atoms (Na-O3D2 and Na-O3C2). At this point the coordination number of the Na atom would increase from six to eight, and it could be argued that the crystal would undergo a *C*2/*c* to *C*2/*c* transition (Chopelas and Serghiou 2002). Procrystal electron density calculations indicate the formation of two additional bond critical points without bond paths at 9.28 GPa, associated with Na-O3D2 and Na-O3C2. Bader (1998) suggested a necessary and sufficient condition for a pair of atoms to be bonded is the existence of a bond path and a bond critical point in the electron density between the pair. Bond formation is therefore predicted at a pressure slightly above 9.28 GPa, when the bond paths fully develop.

In a high-pressure Raman study of diopside, Chopelas and

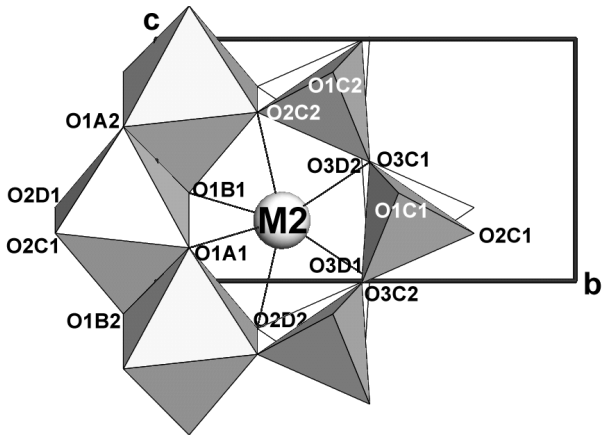

FIGURE 3. Projection of the kosmochlor structure down **a**, showing the bonding around the spherical Na (M2) atom; nomenclature after Burnham et al. (1967). CrO_6 and SiO_4 are depicted as polyhedra. Analysis of the procrystal electron density shows that Na is six-coordinated over the pressure range of this experiment (0–9.28 GPa).

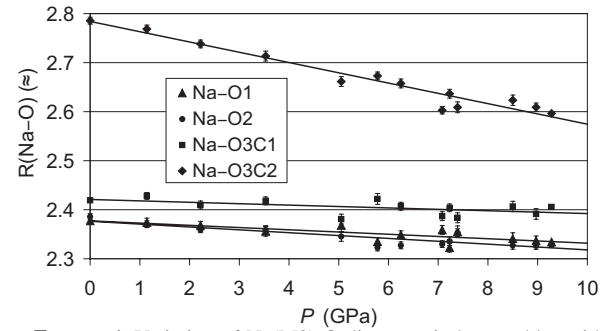

FIGURE 4. Variation of Na(M2)-O distances in kosmochlor with pressure at 298 K.

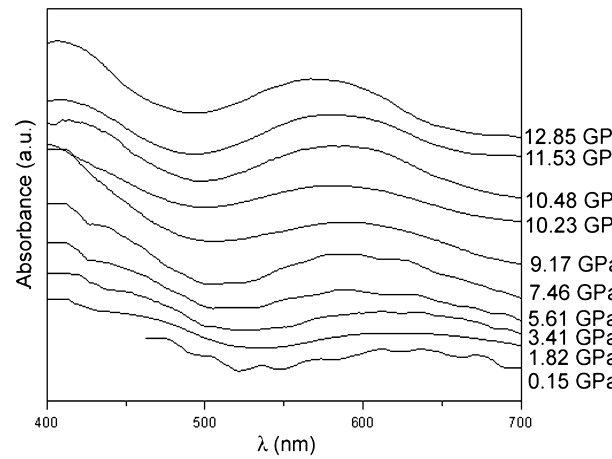

FIGURE 5. Variation of optical absorption spectra of kosmochlor with pressure at 298 K.

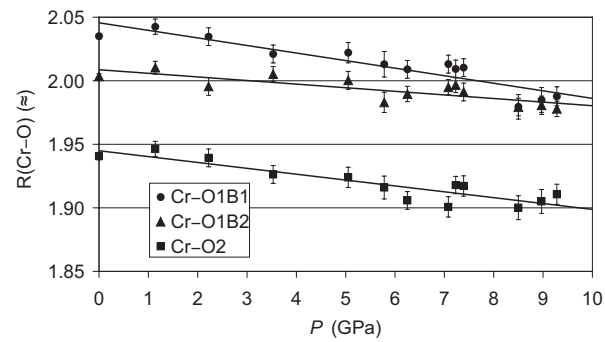

FIGURE 6. Variation of Cr(M1)-O bond lengths in kosmochlor with pressure at 298 K.

Serghiou (2002) observed discontinuities at P = 10.4 GPa in pressure-frequency plots. They suggest that Ca is eight-coordinated below 10.4 GPa, and six-coordinated above 10.4 GPa. Thhey did not observe a symmetry change at this discontinuity, and thus they postulate a $C2/c$ to $C2/c$ phase transition.

Discontinuities in the optical absorption profiles of colored materials have also been attributed to bond formation. For instance, Orgzall et al. (2000) observed a color change from yellow to red in $KTbP_2Se_6$ as a function of pressure, associated with the formation of Se-Se bonds. During the collection of structural data at pressure, we observed a distinct color change from emerald-green to greenish blue in kosmochlor. The color change in kosmochlor might have occurred during the formation of an additional pair of Na-O3 bonds, especially if the formation of the Na-O3 bonds initiates a charge transfer from the CrO_6 octahedron. This would cause a discontinuous and measurable difference in absorption. For this reason, the optical absorption profiles of kosmochlor were collected as function of pressure. Figure 5 is a plot of the absorption profiles of kosmochlor as a function of pressure and shows no discontinuity. The absorption peak center slowly decreases in wavelength, or in other words, increases in energy. This behavior likely results simply from the shortening of Cr-O distances, and the consequent increase in bond energy. As the bond shortens, its electron density increases, and the energy of the bond increases.

Chromium in kosmochlor is coordinated with six O atoms to form a fairly regular octahedron. The Cr is located on a two-fold axis, and there are three distinct pairs of Cr-O bonds. All Cr-O bond lengths decrease with increasing pressure, with the longest distance, R(Cr-O1B1,Cr-O1A1), decreasing twice as rapidly as R(Cr-O1B2, Cr-O1A2) (Fig. 6). Although R(Cr-O1B1) did not fall below R(Cr-O1B2) within this study, linear extrapolation indicates this should occur at ~12 GPa. The average Cr-O bond length varies as R(Cr-O) (Å) = 2.000(3) –0.0044(5)P (GPa). The octahedral volume also decreases systematically with pressure with a bulk modulus $K_0 = 90(16)$ GPa^{-1} with $K' \equiv 4.0$, considerably smaller than the value of 230(30) GPa^{-1} reported by Hazen and Finger (1982) for Cr_2O_3-corundum (Sato and Akimoto 1979). Consideration of octahedral angle variance and quadratic elongation does not reveal any systematic change with pressure, demonstrating that the CrO_6 octahedron does not become more regular with pressure.

The experimental determination of the compressibility of the SiO_4 tetrahedron has been complicated by a lack of sufficient pressure variation, but generally shows a bulk modulus ~300 GPa^{-1} (Hazen and Finger 1982). Analysis of the tetrahedral volumes in Table 4 yield $K_0 = 313(55)$ GPa^{-1} with $K_0' \equiv 4$. The value correlates well with that reported for hedenbergite 347(46) GPa^{-1} (Zhang et al. 1997). However, anomalously low values of $K_0 = 120(25)$, 131(22), 175(48), and 132(52) GPa^{-1} are computed for the tetrahedral volumes in orthorhombic enstatite and $Mg_{0.6}Fe_{0.4}SiO_3$ (Hugh-Jones et al. 1997). The systematic differences between the ortho- and clinopyroxenes are intriguing and warrant further investigation. While the above studies are of sufficient quality to demonstrate meaningful compressibilities of the tetrahedra, the scatter of the values of quadratic elongation reveals no trends involving polyhedral regularity.

In Figure 7, we plot ∠O3-O3-O3 as a function of pressure. The O3-O3-O3 angle defines the extension of the pyroxene silicate chain (Thompson 1970; Cameron et al. 1973). Linear regression gives ∠O3-O3-O3 = 172.6(3)° –0.69(5)P (GPa). The decrease in ∠O3-O3-O3 indicates that the silicate chains are becoming less extended with pressure, or in other words, more kinked. This is an o-type (i.e., opposite) rotation. A $C2/c$ pyroxene with ∠O3-O3-O3 < 180° can be considered distorted cubic closest packed (ccp), and if $\partial\angle$O3-O3-O3/$\partial P < 0$, then it is becoming more ccp with pressure. For diopside and hedenbergite, we calculate slopes of –0.55(7) and –0.51(2) °/GPa, respectively. This slope may indicate how efficiently the structure is approaching ideal ccp. The room condition value of ∠O3–O3–O3, 172.8(2)° in kosmochlor, is higher than that of diopside, 166.37(6)° (Levien and Prewitt 1981), and hedenbergite, 164.4(2)° (Zhang et al. 1997). The room condition values of ∠O3-O3-O3 correlate with their slope, $\partial\angle$O3-O3-O3/∂P, suggesting that the further away the initial structure is from ccp, the more rapidly it approaches ccp with pressure.

A regression of ∠Si-O3-Si against pressure yields the trend ∠Si-O3-Si = 140.0(7) –0.35(10)P (R^2 = 51%). As demonstrated by the R^2 value for this regression, this decrease is not strongly correlated with pressure. The orientation of the crystal in the diamond anvil cell along $(1\bar{1}0)$ aligns Si-O3-Si parallel to the axis of the cell, which explains the relatively larger errors associated with the z-coordinates of Si and O3, and the poor precision of the <Si-O3-Si values.

Zhang et al. (1997) observed that the compressibilities of the CaO_8 and FeO_6 polyhedra in hedenbergite are quite anisotropic. They claimed that the averaged bulk modulus of the CaO_8 and FeO_6 polyhedra, reported as 136 GPa^{-1}, corresponds to the observed bulk modulus of hedenbergite: 117(1) GPa^{-1}. This correspondence in not found in kosmochlor. Assuming a coordination number for Na of six, the average bulk modulus of NaO_6 and AlO_6 is 80 GPa^{-1}, while assuming a coordination number for Na of eight, the average bulk modulus of NaO_8 and AlO_6 is 87 GPa^{-1}. Regardless of the coordination of the M2 site, neither of these values corresponds to the observed bulk modulus of kosmochlor: 134(1) GPa^{-1}.

Furthermore, Zhang et al. (1997) state that "It is the distortion of these [CaO_8 and FeO_6] polyhedra, through their anisotropic compressions in bond lengths, that contributes mainly to the unit-cell compression." As shown above, bond lengths in kosmochlor also change anisotropically. Attempting to characterize the compression mechanisms of pyroxenes through analysis of polyhedral volume changes yields no definitive

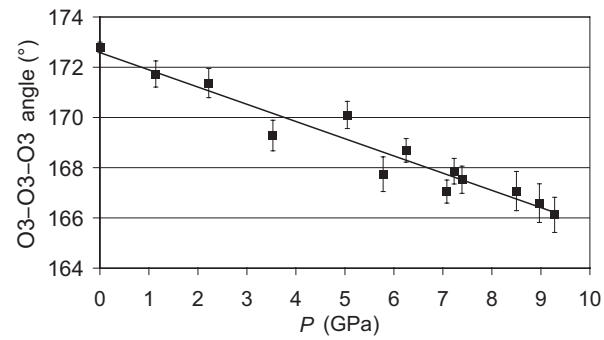

FIGURE 7. Variation of ∠O3-O3-O3 in kosmochlor with pressure at 298 K.

TABLE 4. Selected bond lengths (Å), volumes (Å³), distortion parameters, and angles (°) from structure refinements

P(GPa)	0.0001	1.14	2.22	3.53	5.05	5.78	6.25	7.08	7.23	7.39	8.50	8.97	9.28
R(Na-O1)	2.377(3)	2.374(7)	2.368(9)	2.356(8)	2.368(10)	2.335(14)	2.349(8)	2.359(8)	2.323(9)	2.355(9)	2.341(12)	2.337(10)	2.334(10)
R(Na-O2)	2.386(2)	2.371(6)	2.359(7)	2.359(6)	2.346(8)	2.323(10)	2.327(7)	2.330(7)	2.336(7)	2.353(9)	2.327(8)	2.326(8)	2.328(7)
R(Na-O3)	2.419(3)	2.428(7)	2.410(8)	2.418(8)	2.381(10)	2.422(11)	2.407(8)	2.387(9)	2.404(8)	2.384(10)	2.407(10)	2.392(11)	2.406(9)
R(Na-O3)	2.786(3)	2.769(7)	2.738(8)	2.713(8)	2.661(10)	2.673(10)	2.658(8)	2.603(9)	2.637(7)	2.609(9)	2.623(11)	2.609(11)	2.596(8)
<R(Na-O)>	2.425(5)	2.391(4)	2.379(5)	2.378(4)	2.420(4)	2.360(7)	2.361(4)	2.468(6)	2.354(5)	2.439(5)	2.358(6)	2.352(6)	2.356(5)
R(Cr-O1)	2.035(2)	2.043(6)	2.035(7)	2.021(7)	2.022(8)	2.013(10)	2.009(7)	2.013(7)	2.009(7)	2.010(7)	1.979(10)	1.985(10)	1.988(7)
R(Cr-O1)	2.003(2)	2.010(5)	1.996(7)	2.005(6)	2.000(7)	1.983(8)	1.990(6)	1.995(6)	1.997(6)	1.991(7)	1.979(7)	1.981(7)	1.978(6)
R(Cr-O2)	1.941(3)	1.946(6)	1.939(7)	1.926(7)	1.924(8)	1.916(9)	1.906(7)	1.901(8)	1.918(7)	1.917(8)	1.900(9)	1.905(9)	1.911(8)
< R(Cr-O)>	1.993(4)	2.000(3)	1.990(4)	1.984(4)	1.982(4)	1.971(5)	1.968(4)	1.970(6)	1.975(4)	1.973(4)	1.953(5)	1.957(5)	1.959(4)
$V(CrO_6)$	10.422	10.542	10.385	10.298	10.277	10.091	10.052	10.083	10.149	10.118	9.809	9.873	9.899
Cr q.e.*	1.0090	1.0080	1.0081	1.0080	1.0073	1.0080	1.0080	1.0075	1.0081	1.0084	1.0088	1.0084	1.0085
<Si-O>	1.627(1)	1.625(3)	1.618(4)	1.617(3)	1.617(4)	1.613(5)	1.614(4)	1.617(4)	1.613(3)	1.614(4)	1.613(5)	1.612(5)	1.609(4)
$V(SiO_4)$	2.196	2.189	2.162	2.158	2.158	2.143	2.147	2.157	2.143	2.151	2.141	2.141	2.130
Si q.e.*	1.0040	1.0040	1.0040	1.0032	1.0046	1.0037	1.0040	1.0038	1.0029	1.0027	1.0034	1.0033	1.0027
O3-O3-O3	172.8(2)	171.7(5)	171.4(6)	169.3(6)	170.1(5)	167.7(7)	168.7(5)	167.1(5)	167.9(5)	167.5(5)	167.1(8)	166.6(8)	166.1(7)
Si-O3-Si	140.2(2)	140.1(5)	138.9(6)	139.4(5)	136.2(8)	139.4(8)	138.7(7)	135.9(7)	137(6)	136.3(8)	138.1(7)	137.2(7)	137.3(5)

* Quadratic elongation after Robinson et al. (1971).

solutions. For instance, at the octahedral M1 site, divalent Fe^{2+} in hedenbergite results in a larger bulk modulus, 149(4) GPa^{-1}, than the trivalent Cr^{3+} in kosmochlor, 90(16) GPa^{-1}. This contradicts any reasonable compression model based upon polyhedral systematics, since the cation with larger valence should have stronger bonds that are more resistant to compression.

Thompson and Downs (2001) suggest that many structures with distorted closest packed arrangements of anions become more closest packed with pressure. They show that diopside, fassaite, ferrosilite, hedenbergite, and kanoite become more closest packed with pressure, and suggest that this tendency drives the observed angle bending and bond compression systematics. In order to quantify the distortion of an anion array from closest packing, Thompson and Downs (2001) defined the parameter U_{cp} which is a measure of the isotropic mean-square displacement of anions from their ideal closest packed equivalent positions. As a structure moves toward closest packing, the value of U_{cp} decreases. Figure 8 is a plot of U_{cp} as a function of pressure for kosmochlor, and demonstrates that this structure becomes significantly more closest packed with pressure. Above we suggest a correlation between $\partial\angle$O3-O3-O3/∂P and the tendency toward closest packing with pressure. The value $\partial U_{cp}/\partial P$ quantifies the tendency toward closest packing with pressure. We determine the value $\partial U_{cp}/\partial P$ for kosmochlor and values for diopside and hedenbergite are from Thompson and Downs (2001). Below, the correlation between $\partial U_{cp}/\partial P$, $\partial\angle$O3-O3-O3/∂P, and $\angle$O3-O3-O3 for P = 1 atm is indicated:

	$\partial U_{cp}/\partial P$	$\partial\angle$O3-O3-O3/∂P	$\angle$O3-O3-O3$_0$
hedenbergite	–0.0136	–0.51(2)	164.4(2)°
diopside	–0.0173	–0.55(7)	166.37(6)°
kosmochlor	–0.0196	–0.69(5)	172.8(2)°

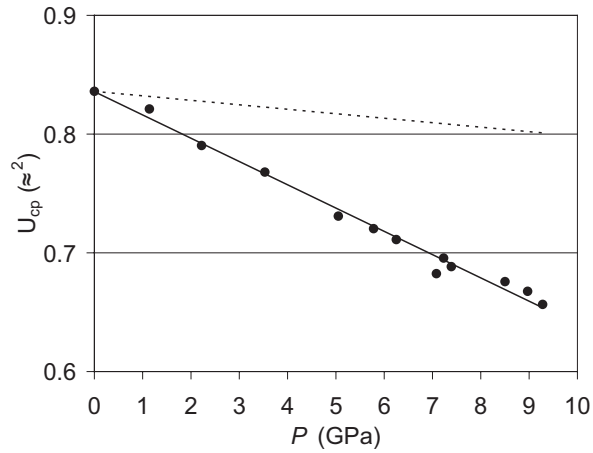

FIGURE 8. Plot of the isotropic closest packed distortion parameter, U_{cp}, as defined by Thompson and Downs (2001) vs. pressure for kosmochlor. U_{cp} is a measure of the average displacement of the anions from a perfectly close packed arrangement. Filled symbols represent U_{cp} calculated from observed structural data. The solid line represents a linear fit to the data and the dashed line represents the decrease in distortion due to scaling of the structure without changing atomic positions. This figure shows that the kosmochlor structure is becoming more closest packed with pressure.

Anisotropic compression in pyroxene

As indicated above, the compressibility of kosmochlor is anisotropic, with axial ratios of the strain ellipsoid: 1:1.82:2.08. Zhang et al. (1997) noted that both diopside and hedenbergite undergo anisotropic compression, however they only examined axial compressibilities, without the aid of unit strain ellipsoids. We examined the pressure behavior of several pyroxenes and found a common and systematic tendency toward anisotropic compression. A search of the literature yielded cell parameter data for each of the major pyroxene topologies as a function of pressure, with space groups $C2/c$, $P2_1/c$, $Pbca$, $Pbcn$, and $P2_1cn$. Strain ellipsoids were computed with Ohashi's STRAIN software, and are listed in Table 5. The most anisotropic compression is found for hedenbergite with the ratio 1:3.25:2.98, and the least anisotropic is found for orthoenstatite with the ratio 1:1.24:1.60.

The anisotropy of pyroxene compression may be understood in terms of a closest packing model. As mentioned earlier, the kosmochlor structure can be modeled as a distorted cubic closest packed arrangement of O atoms. In the ideal cubic closest packed pyroxene structure, there are four directions of stacking: (100), ($\bar{1}$01), (131), and (1$\bar{3}$1) (Thompson and Downs, in preparation). The most compressible direction in kosmochlor correlates with one of the stacking directions of O atom monolayers. Using the room condition cell parameter data (from Table 1), the distances between monolayers for these directions are found to be 2.282 Å, 2.548 Å, 2.335 Å, and 2.335 Å, respectively. Of these four directions, the direction with the largest interlayer spacing is ($\bar{1}$01), which closely matches the observed most compressible direction in kosmochlor of ($\bar{3}$02), as illustrated in Figure 2. The least compressible direction is ~(201). It is not possible to align two of the three orthogonal axes of a strain ellipsoid with two stacking directions of a ccp array since the stacking directions are either 70.53° or 109.47° apart. These two contributions compete to determine the orientation of the strain ellipsoid.

Levien and Prewitt (1981) studied the compression of diopside. They noted that the most compressible direction is **b**. Equally significant is the next most compressible direction ($\bar{3}$02), since the strain ellipsoid is essentially a circular section through the crystal, with unit strain values of –0.00326(6) GPa^{-1} and –0.00327(6) GPa^{-1} for ($\bar{3}$02) and (010), respectively. Extending our O atom packing approach to diopside, and using the diopside cell data for 1 atm from Levien and Prewitt (1981), we calculate the interlayer spacing of the stacking directions of (100), ($\bar{1}$01), (131), and (1$\bar{3}$1) as 2.344, 2.531, 2.389, and 2.389 Å, respectively. The most compressible direction in diopside is observed to be ~($\bar{3}$02) and the least compressible direction ~(201). Consequently, compression in diopside is similar to that in kosmochlor and may also be regulated by anion-anion repulsion.

Tribaudino et al. (2000, 2001) discussed compression mechanisms in members of the diopside-enstatite series. They related observed compression effects to shearing of the tetrahedral chains, which they suggest will reduce the volume of the M2 polyhedron and increase its regularity. Once M2-O3

TABLE 5. Unit strain ellipsoid parameters for various pyroxenes

Pyroxene	Symmetry	ΔP	Unit-strain ellipsoid axes (GPa^{-1}) ($\times -10^2$)			Orientation	Source
			ε_1	ε_2	ε_3	$\angle(\varepsilon_3 \wedge \mathbf{c})$	
kosmochlor	*C2/c*	0–9.28	0.1407(6)	0.2556(5)	0.2930(5)	32.1(1)	this study
diopside	*C2/c*	0–5.30	0.144(4)	0.327(6)	0.326(6)	37(1)	Levien and Prewitt (1981)
diopside	*C2/c*	0–9.34	0.129(3)	0.320(1)	0.316(2)	35.4(6)	Zhang et al. (1997)
hedenbergite	*C2/c*	0–9.34	0.102(2)	0.332(1)	0.304(2)	30.5(4)	Zhang et al. (1997)
spodumene	*C2/c*	0–3.16	0.148(6)	0.242(4)	0.258(3)	50(2)	Artl and Angel (2000)
$LiScSi_2O_6$	*C2/c*	0–0.30	0.17(3)	0.28(3)	0.45(2)	52(3)	Artl and Angel (2000)
high-*P* clinoenstatite	*C2/c*	5.34–7.93	0.11(2)	0.280(6)	0.28(1)	44(3)	Angel and Hugh-Jones (1994)
spodumene	$P2_1/c$	3.34–8.84	0.165(1)	0.209(2)	0.319(1)	16.3(4)	Artl and Angel (2000)
$LiScSi_2O_6$	$P2_1/c$	0.66–4.80	0.235(2)	0.269(2)	0.534(1)	31.1(2)	Artl and Angel (2000)
clinoenstatite	$P2_1/c$	0–6.98	0.140(9)	0.310(5)	0.293(5)	35(1)	Angel and Hugh-Jones (1994)
orthoenstatite	*Pbca*	0–8.51	0.191(1)	0.236(2)	0.306(2)	0	Hugh-Jones and Angel (1994)
$Mg_{1.54}Li_{.23}Sc_{.23}Si_2O_6$	*Pbcn*	0–2.03	0.184(4)	0.237(4)	0.306(13)	0	Yang et al. (1999)
$Mg_{1.54}Li_{.23}Sc_{.23}Si_2O_6$	$P2_1cn$	2.50–9.98	0.200(2)	0.344(4)	0.198(1)	0	Yang et al. (1999)

Note: Strain ellipsoids are symmetrically constrained to lie with $e_2 \| \mathbf{b}$ and $\angle(\varepsilon_1 \wedge b) = \angle(\varepsilon_3 \wedge b) = 90°$; $\angle(\varepsilon_1 \wedge c) = 90° - \angle(\varepsilon_3 \wedge c)$, $\angle(\varepsilon_1 \wedge a) = 90° - \angle(\varepsilon_3 \wedge a)$; $\angle(e_3 \wedge a) = \angle(e_3 \wedge c) + \beta(107.5°)$.

bonds achieve similar dimensions at ~5GPa, they suggest that the compression mechanism of the pyroxene changes, using extrapolated structural data. However, the data for kosmochlor do not indicate an increase in regularity of the M2 polyhedron.

Hedenbergite has interlayer spacings 2.378, 2.520, 2.417, and 2.417 for (100), $(\bar{1}01)$, (131), and $(1\bar{3}1)$, respectively. The smallest spacing is in the (100) direction, while the largest spacing is in the $(\bar{1}01)$ direction. The most compressible direction is ~$(\bar{3}02)$ and the least compressible is ~(201). This also follows the compression systematic observed in kosmochlor and diopside.

Examination of the unit strain ellipsoids of *C*2/*c* pyroxenes separates them into two distinct groups, based on orientation. Those with angle $\angle(\varepsilon_3 \wedge \mathbf{a}) \sim 40°$ include kosmochlor, diopside, and hedenbergite, while another group with $\angle(\varepsilon_3 \wedge \mathbf{a})$ ~20° includes spodumene and $LiScSi_2O_6$. The first group of pyroxenes has cations of varying valence and size, Na and Ca at M1 and Fe^{2+}, Mg, and Cr at M2. Varying valence of the M1 and M2 cations does not affect the direction of maximum compressibility in these phases. Additionally, the change in coordination of the M2 site from six-coordinate Na or eight-coordinate Ca does not alter the direction of maximum compressibility. As these structures exhibit a common direction of maximal compressibility, and share similar O atom stacking arrangements, the anions appear to dominate the compression behavior.

The second group of *C*2/*c* pyroxenes with $\angle(\varepsilon_3 \wedge \mathbf{a})$ ~20° contain Li at the M2 site. Since spodumene has a room condition ∠O3-O3-O3 > 180°, it can be argued that its O atoms adopt a distorted hexagonal closest packing arrangement, and therefore have only one stacking direction parallel to **a***. This may explain the change in orientation of the unit strain ellipsoid as shown in Figure 9. Spodumene and $LiScSi_2O_6$ both display the most compressible direction ~$(\bar{3}01)$ and least compressible direction ~(101).

We examined three structures with $P2_1/c$ symmetry, spodumene, $LiScSi_2O_6$, and clinoenstatite. The orientation of the unit strain ellipsoid for spodumene (Fig. 9) differs from that for $LiScSi_2O_6$ and clinoenstatite. However, Downs (2003) suggests that there is a bonding change in spodumene in the interval over which the unit strain ellipsoid is computed which may affect its orientation. The *C*2/*c* to $P2_1/c$ transition in spodumene changes the orientation of unit strain ellipsoid, while the $P2_1/c$ to *C*2/*c* transition in clinoenstatite does not change the orientation. The most incompressible direction of the unit strain ellipsoid for $P2_1/c$ spodumene approximates the **a*** stacking direction (Fig. 10).

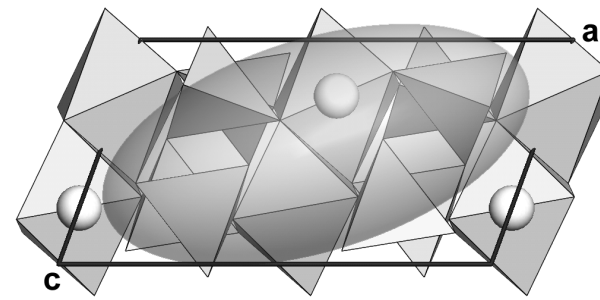

FIGURE 9. Oriented unit strain ellipsoid for *C*2/*c* spodumene (0–3.164 GPa) overlying a cartoon of the spodumene structure viewed down **b**. Spodumene and $LiScSi_2O_6$ have their most compressible directions ~$(\bar{3}01)$ while the least compressible direction ~(101).

Orthorhombic pyroxenes are constrained to compress with the axes of the strain ellipsoid parallel to crystallographic axes. Orthorhombic pyroxenes have only one stacking direction, **a***. The orthorhombic pyroxenes listed in Table 5 represent three space groups, *Pbca, Pbcn,* and $P2_1cn$, and all have their least compressible direction parallel to the stacking vector **a***, similar to $P2_1/c$ spodumene, as illusstrated in Fig. 11. Over the *Pbcn* to $P2_1cn$ transition in $Mg_{1.54}Li_{.23}Sc_{.23}Si_2O_6$, the most compressible direction switches from **b** to **c**.

Relationship between compressional anistropies of olivine and pyroxene

With movement of pyroxene and olivine crystals through a convecting mantle, crystals may align with their least compressible directions normal to the stress field. The most incompressible direction in forsterite (olivine) is (100) and the most incompressible direction in clinoenstatite is ~(302), in diopside is ~(201), and in orthoenstatite is (100). We predict the following relationships between the crystallographic axes of

olivine and pyroxene in a stress field: $(100)_{olivine} \parallel (302)_{clinoenstatite} \parallel (201)_{diopside} \parallel (100)_{orthoenstatite}$. Analysis of exhumed mantle terrains should show a correlation of pyroxene and olivine orientations, which could provide additional constraints on the metamorphic history of these rocks. Furthermore, due to the differences in the magnitudes of the compressibilities of olivine and pyroxene, it may be possible to estimate the magnitude of the stress fields.

ACKNOWLEDGMENTS

This study was supported by the National Science Foundation grant for the study of Compression Mechanisms of Upper Mantle Minerals, EAR-9903104.

REFERENCES CITED

Anthony, J.W., Bideaux, R.A., Bladh, K.W., and Nichols, M.C. (1995) Handbook of Mineralogy. Volume II: Silica, silicates. Part one, page 430. Mineral Data Publishing, Tucson, Arizona.

Angel, R.J. and Hugh-Jones, D.A. (1994) Equations of state and thermodynamic properties of enstatite pyroxenes. Journal of Geophysical Research, 99, B10, 19777–19783.

Arlt, T. and Angel, R.J. (2000) Displacive phase transitions in C-centred clinopyroxenes: spodumene, $LiScSi_2O_6$ and $ZnSiO_3$. Physics and Chemistry of Minerals, 27, 719–731.

Bader, R.F.W. (1998) A bond path: a universal indicator of bonded interactions. Journal of Physical Chemistry, 102A, 7314–7323.

Burnham, C.W., Clark, J.R., Papike, J.J., and Prewitt, C.T. (1967) A proposed crystallographic nomenclature for clinopyroxene structures. Zeitschrift für Kristallographie, 125, 109–119.

Cameron, M. and Papike, J.J. (1981) Structural and chemical variations in pyroxenes. American Mineralogist, 66, 1–50.

Cameron, M., Sueno, S., Prewitt, C.T., and Papike, J.J. (1973) High-temperature crystal chemistry of acmite, diopside, hedenbergite, jadeite, spodumene, and ureyite. American Mineralogist, 58, 594–618.

Chopelas, A. and Serghiou, G. (2002) Spectroscopic evidence for pressure-induced phase transitions in diopside. Physics and Chemistry of Minerals, 29, 403–408.

Clark, J.R., Appleman, D.E., and Papike, J.J. (1969) Crystal-chemical characterization of clinopyroxenes based on eight new structure refinements. Mineralogical Society of America Special Paper 2, 31–50.

Downs, R.T. (2003) Topology of the pyroxenes as a function of temperature, pressure and composition determined from the procrystal electron density. American Mineralogist, 88, 556–566.

Downs, R.T., Gibbs, G.V., Boisen, M.B. Jr., and Rosso, K.M. (2002) A comparison of procrystal and ab initio representations of the electron-density distributions of minerals. Physics and Chemistry of Minerals, 29, 369–385.

Downs, R.T. and Hall-Wallace, M. (2003) The American Mineralogist crystal structure database. American Mineralogist, 88, 247–250.

Downs, R.T., Zha, C.-S., Duffy, T.S., and Finger, L.W. (1996) The equation of state of forsterite to 17.2 GPa and effects of pressure media. American Mineralogist, 81, 51–55.

Finger, L.W. and Prince, E. (1975) A system of Fortran IV computer programs for crystal structure computations. U S Bureau of National Standards Technical Note 854, 128 pp.

Frondel, C. and Klein, C. Jr. (1965) Ureyite, $NaCrSi_2O_6$, a new meteoritic pyroxene. Science, 149, 742–744.

Hamilton, W.C. (1959) On the isotropic temperature factor equivalent to a given anisotropic temperature factor. Acta Crystallographica, 12, 609–610.

Harlow, G.E. (1997) K in clinopyroxene at high pressure and temperature: An experimental study. American Mineralogist, 82, 259–269.

Harlow, G.E. and Olds, E.P. (1987) Observations on terrestrial ureyite and ureyitic pyroxene. American Mineralogist, 72, 126–136.

Hazen, R.M. and Finger, L.W. (1982) Comparative crystal chemistry. John Wiley & Sons, New York, New York, 231 pp.

Hazen, R.M., Downs, R.T., and Prewitt, C.T. (2000) Principles of comparative crystal chemistry. In R.M. Hazen and R.T. Downs, Eds., High-temperature and high-pressure crystal chemistry, p. 1–33. Reviews in Mineralogy and Geochemistry, volume 41, Mineralogical Society of America and the Geochemical Society, Washington, D.C.

Hugh-Jones, D.A. and Angel, R.J. (1994) A compressional study of $MgSiO_3$ orthoenstatite up to 8.5 GPa. American Mineralogist, 79, 405–410.

Hugh-Jones, D., Sharp, T., Angel, R., and Woodland, A. (1996) The transition of orthoferrosilite to high-pressure *C*2/*c* clinoferrosilite at ambient temperature. European Journal of Mineralogy, 8, 1337–1345.

Hugh-Jones, D.A., Chopelas, A., and Angel, R.J. (1997) Tetrahedral compression in $(Mg,Fe)SiO_3$ orthopyroxenes. Physics and Chemistry of Minerals, 24, 301–310.

Ibers, J.A. and Hamilton, W.C., Eds. (1974) International Tables for X-ray Crystallography, Vol IV, 366 p. Kynoch Press, Birmingham, U.K.

Jung, H. and Karato, S. (2001) Water-induced fabric transitions in olivine. Science, 293, 1460–1463.

King, H.E. Jr. and Finger, L.W. (1979) Diffracted beam crystal centering and its application to high-pressure crystallography. Journal of Applied Crystallography, 12, 374–378.

Laspeyres, H. (1897) Die steinigen Gemengtheile im Meteoreisen von Toluca in Mexico. Zeitschrift für Krystallographie und Mineralogie, 27, 586–600.

Levien, L. and Prewitt, C.T. (1981) High pressure structural study of diopside. American Mineralogist, 66, 315–323.

Mao, H.K., Bell, P.M., Shaner, J.W., and Steinberg, D.J. (1978) Specific volume measurements of Cu, Mo, Pd, and Ag and calibration of the ruby R_1 fluorescence pressure gauge from 0.06 to 1 Mbar. Journal of Applied Physics, 49, 3276–3283.

Morimoto, N., Fabries, J., Ferguson, A.K., Ginzburg, I.V., Ross, M., Seifert, F.A., Zussman, J., Aoki, K., and Gottardi, G. (1988) Nomenclature of pyroxenes. American Mineralogist, 73, 1123–1133.

Neuhaus, A. (1967) Über Kosmochlor (Ureyit). Naturwissenschaften, 54, 440–441.

Orgzall, I., Lorenz, B., Dorhout, P.K., Van Calcar, P.M., Brister, K., Sander, T., and Hochheimer, H.D. (2000) High pressure optical and X-ray diffraction studies of two polymorphs of $K(RE)P_2Se_6$ (RE = Pr and Tb). Journal of Physics and Chemistry of Solids, 61, 123–134.

Papike, J.J., Prewitt, C.T., Sueno, S., and Cameron, M. (1973) Pyroxenes: comparisons of real and ideal structural topologies. Zeitschrift für Kristallographie, 138, 254–273.

Robinson, K., Gibbs, G.V., and Ribbe, P.H. (1971) Quadratic elongation: a quantitative measure of distortion in coordination polyhedra. Science, 172, 567–570.

Sato, Y. and Akimoto, S. (1979) Hydrostatic compression of four corundum-type compounds: a-Al_2O_3, V_2O_3, Cr_2O_3, and a-Fe_2O_3. Journal of Applied Physics, 50, 5285–5291.

Secco, L., Martignago, F., Dal Negro, A., Reznitskii, L.Z., and Sklyarov, E.V. (2002) Crystal chemistry of Cr^{3+}-V^{3+}-rich clinopyroxenes. American Mineralogist, 87, 709–714.

Thompson, J.B. Jr. (1970) Geometrical possibilities for amphibole structures: model biopyriboles. American Mineralogist, 55, 292–293.

Thompson, R.M. and Downs, R.T. (2001) Quantifying distortion from ideal closest-packing in a crystal structure with analysis and application. Acta Crystallographica, B57, 119–127.

Thompson, R.M. and Downs, R.T. (2003) Model pyroxenes I: Ideal pyroxene topologies. American Mineralogist, 88, 653–666.

Tribaudino, M., Prencipe, M., Bruno, M., and Levy, D. (2000) High-pressure behaviour of Ca-rich C2/c clinopyroxenes along the join diopside-enstatite ($CaMgSi_2O_6$-$Mg_2Si_2O_6$). Physics and Chemistry of Minerals, 27, 656–664.

Tribaudino, M., Prencipe, M., Nestola, F., and Hanfland, M. (2001) A $P2_1/c$-C2/c high-pressure phase transition in $Ca_{0.5}Mg_{1.5}Si_2O_6$ clinopyroxene. American Mineralogist, 86, 807–813.

Yang, H. and Prewitt, C.T. (2000) Chain and layer silicates at high temperatures and pressures. In R.M. Hazen and R.T. Downs, Eds., High-temperature and high-pressure crystal chemistry, p. 211-255. Reviews in Mineralogy and Geochemistry, volume 41, Mineralogical Society of America and the Geochemical Society, Washington, D.C.

Yang, H., Finger, L.W., Conrad, P.G., Prewitt, C.T., and Hazen, R.M. (1999) A new pyroxene at high pressure: Single-crystal X-ray and Raman study of the *Pbcn*-$P2_1cn$ phase transition in protopyroxene. American Mineralogist, 84, 245–256.

Zhang, L., Ahsbahs, H., Hafner, S.S., and Kutoglu, A. (1997) Single-crystal compression and crystal structure of clinopyroxene up to 10 GPa. American Mineralogist, 82, 245–248.

MANUSCRIPT RECEIVED SEPTEMBER 24, 2002
MANUSCRIPT ACCEPTED DECEMBER 23, 2002
MANUSCRIPT HANDLED BY ALISON PAWLEY